Available online at www.garmian.edu.krd

Passer Journal

Passer 4 (Issue 2) (2022) 135-143

http://passer.garmian.edu.krd/

Classification of COVID-19 on Chest X-Ray Images Through the Fusion of HOG and LPQ Feature Sets

Rebin Abdulkareem Hamaamin[1*], Shakhawan Hares Wady[1],Ali Wahab Kareem[2]

[1]*Applied Computer, Medicals and Applied Sciences, Charmo University, Kurdistan Region, Iraq*
[2]*General Science, Education and Language, Charmo University, Kurdistan Region, Iraq*

Received 17 April 2022; revised 19 August 2022;
accepted 20 August 2022; available online 23 August 2022

doi:10.24271/psr.51

ABSTRACT

Covid-19 is a contagious disease that affects people's everyday life, personal health, as well as a nation's economy. COVID-19 infected individuals, according to a clinical study, are most usually contaminated with a severe condition after coming into a primary infection. The chest radiograph (also known as the chest X-ray or CXR) or a chest CT scan is a more reliable imaging method for diagnosing COVID-19 infected individuals. This article proposed a novel technique for classifying CXR scan images as healthy or affected COVID-19 by fusing the features extracted using Histogram of Oriented Gradient (HOG) and Local Phase Quantization (LPQ). This research is an experimental study that employed 7232 CXR images from a COVID-19 Radiography dataset as training and testing data. As a result, by using both individual and fused feature extraction methodologies, a developed model was created and fed into the machine learning techniques. The testing results reveal that the improved architecture outperforms current methods for identifying COVID-19 patients in terms of accuracy rate, which reached 97.15 %.

Keywords: COVID-19, CXR images, feature extraction, machine learning, image classification.

1. Introduction

A new ailment caused by a coronavirus first arose in China's Hubei province at the end of 2019 and quickly expanded worldwide in 2020. In February 2020, the World Health Organization (WHO) designated this illness as COVID-19. The infectious disease known as Coronavirus disease (COVID-19) is brought on by the virus SARS-CoV-2. Most COVID-19 patients will experience mild to severe symptoms and will recover on their own without any kind of treatment. Others, on the other hand, will become extremely unwell and require urgent medical attention[1]. The disease quickly spread throughout China and to many other countries after the first confirmed COVID19 case was found in Wuhan City. The entire world has worked and fought to stop this virus from spreading[2]. The medical criteria for the diagnosis of COVID-19 include the following symptoms: fever, tiredness, chronic cough, sore throat, diarrhea, blue lips or a blue face, shortness of breath, loss of smell, anorexia, exhaustion, headache, myalgia, anosmia, and dyspnea[3].

* Corresponding author
E-mail address: rebin.abdulkarim@charmouniversity.org (Instructor).
Peer-reviewed under the responsibility of the University of Garmian.

Patients who have COVID-19 will mostly experience symptoms in the upper and lower respiratory tract, necessitating the use of ventilators and other hospital treatment. For many years, CXR images have been used to track and assess a range of lung conditions, such as malignancy, herniation, dilatation, pneumonia, and infiltrates[4]. The two most popular imaging studies for diagnosing and managing COVID-19 patients are CXR and chest CT. Chest radiography and CT scans, on the other hand, are widely available at most medical centers, are routinely obtained, and are typically interpreted with a faster turnaround time than the SARS-CoV-2 laboratory testing[2]. To identify COVID-19 patients, numerous studies are focusing on the use of Artificial Intelligence (AI) technologies, Machine Learning (ML), and Deep Learning (DL) approaches[5, 6].

The primary goal of this study is the development of a Computer Aided Diagnosis (CAD) system to categorize and diagnose COVID-19, and it investigates the impact of several feature approaches on the classification procedure. This paper's main contribution is the fusion of the features taken from CXR images to increase overall performance and lower the misclassification error rate. The remainder of the Paper is divided into the following sections: Section two provides an overview of the

related work background. Section three depicts materials and methods used in the study including research design, COVID-19 dataset description, image preprocessing, feature extraction feature fusion, and classifier and performance metrics. Discussion of Experiment Results summarized in Section four. Finally, section five discusses the conclusion of the present study.

2. Related Works

Numerous investigations on COVID-19 infection diagnosis and detection have been conducted over the previous two years. For instance, the authors of[7] offered a pertained Convolutional Neural Network (CNN) based on the AlexNet model employing the transfer learning technique that was deployed for this objective. The Support Vector Machine (SVM) technique was performed to classify the effective features selected by the Relief feature selection procedure at all levels of the architecture. Tayyaba Ilyas[8] suggested for COVID-19 detection, it is proposed to offer a real time rule based Fuzzy Logic classifier (FLCD). The suggested methodology collects real-time symptom data from users through the use of an Internet of Things (IoT) platform to identify symptomatic and asymptomatic COVID-19 patients.

The authors in[6] concentrated on potential COVID-19 vaccination efficacy predictions, which were represented as a glimmer of light in the darkness. People are concerned about a variety of issues, along with the COVID-19 vaccine's effectiveness. For estimating the general predisposition toward the COVID-19 vaccine, five models were performed: Artificial Neural Network (ANN), Random Forest (RF), SVM, K-Nearest Neighbor (KNN), and Decision Tree (DT). In[9], optimal ML models were applied on the publicly available dataset to determine certain particular quantifiable host indicators connected to COVID-19 disease. Upon the dataset, the two potent feature selection techniques Minimum Redundancy and Maximum Relevance (mRMR) were used. The Incremental Feature Selection (IFS) methodology was then used to choose features from the resulting feature list. In the IFS method, four conventional categorization algorithms were employed. In order to differentiate COVID-19 individuals from patients with normal, viral pneumonia, and bacterial pneumonia, a deep CNN-based technique was developed in[10]. The implementation of nine pre-trained CNN schemas to investigate transfer learning approaches resulted in the discovery that fine-tuning the pre-trained CNN schemas can be effectively employed to a small sample dataset.

The authors in[11] recommended a framework for determining COVID-19 patients' prognosis based on patient indicators tracked at home throughout quarantine. A set of 287 COVID-19 examples were collected from patients at Saudi Arabia's King Fahad University Hospital. Three different classification methods were utilized to evaluate the collected dataset: Logistic Regression (LR), RF, and Extreme Gradient Boosting (XGB). Alireza Davoudi et al. in[12] observed the influence of utilizing regular doses of statins in the months preceding infection in COVID-19 patients admitted to the hospital. In the study, ML algorithms including Naive Bayes (NB), DT, KNN, SVM, and Discriminant Analysis classifiers were performed to identify the severity of COVID-19 patients depending on clinical features. In this respect also the work presented in[13] recommended a COVID-19 infection recognition procedure using CXR images. To collect and select significant features from CXR images, the Hybrid Social Group Optimization (HSGO) strategy was utilized. The selected set features were then passed into the classification techniques that used SVM and DL techniques to categorize the CXR images. The authors in[14] proposed a new testing methodology to determine whether a patient has been infected by COVID-19 virus using the SDD300 model. The deep feature plus SVM based procedure was proposed in[15] for identifying coronavirus infected patients by applying X-ray images. SVM was utilized for classification rather than deep learning-based classifiers, which require a large dataset for training and validation.

In[16], The authors recommended five pre-trained CNN architectures including Inception-ResNetV2, InceptionV3, ResNet50, ResNet101, and ResNet152 for identifying patients with COVID-19 pneumonia utilizing CXR radiographs. An innovative concept of cluster based one shot learning was introduced in[17] for categorizing images into four sorts: normal, pneumonia virus, pneumonia bacterial, and COVID-19 cases. In contrast to deep learning architectures, the introduced approach offered the advantage of learning from a few examples rather than many samples. An ensemble of Generalized Regression Neural Network (GRNN) and Probabilistic Neural Network (PNN) classifiers was used to generate the recommended multi-class classification algorithm at the decision level. Based on image modal feature fusion, the authors in[18] presented a COVID-19 detection approach. Small-sample enhancement preprocessing, including as spinning, translation, and randomized transformation, was initially conducted using this methodology. Five classic pre training models including VGG19, ResNet152, Xception, DenseNet201, and InceptionResnetV2 were utilized to extract the features from CXR images. For classifying CXR images into pneumonia, COVID-19, and normal patients, the authors of[19] suggested a new CNN and Deep Convolutional Generative Adversarial Networks (DCGANs) approach. The designed scheme, comprised of two fully interconnected layers, four max-pooling layers, and eight convolutional layers, performed significantly better than traditional pre-trained methodologies (AlexNet and GoogLeNet). By analyzing CXR images[20], provided deep and transfer learning strategies to distinguish COVID-19 instances. To effectively utilize their potential, the designed methods used either CNN or transfer learning frameworks, or hybridize them with sophisticated ML algorithms.

To tackle the inconsistencies in the previous COVID-19 classification methods, the study of[21] proposed combining a Moment Invariant (MI) technique and a DL procedure for feature extraction tasks. Through using the cascade fusion method, the suggested scheme combined MI-based features into DL models. The integration of MI and DL features was revealed to have the potential to increase the COVID-19 classification's sensitivity and accuracy. By combining the features derived by the Gabor Wavelet Transform (GWT), Curvelet Transform (CT), and Local Gradient Increasing Pattern (LGIP), the authors in[22] developed and created an automated workflow for COVID-19 identification. Four ML classifiers were used to process the retrieved features

from CXR images: Discriminant Analysis, Ensemble, RF, and SVM classifiers. In the study of[23], deep feature extraction, pretrained CNN fine tuning, and end to end training of a designed CNN framework were utilized to identify COVID-19 and regular CXR images. Deep CNN systems (VGG16, VGG19, ResNet18, ResNet50, and ResNet101) were employed for deep feature extraction. In addition, SVM classifier with numerous kernel functions, such as Linear, Quadratic, Cubic, and Gaussian, was computed to categorize the deep features.

This study developed an intelligent schema to identify COVID-19 as positive (CXR+) or negative (CXR−) cases. The framework uses HOG and LPQ descriptor methods for feature extraction process. A uniform dataset with 7232 CXR images was used as testing and training set. Furthermore, a recommended schema was built by employing different classifiers such as KNN, Ensemble, DT, NB, and SVM.

3. Materials and Methods

3.1 Research Design

A sequence of experimental and analytical studies was adopted on CXR images as input data to fulfill the objective of the present study. To begin, this methodology transformed RGB images to grayscale and then removed non-interesting regions to determine the Region of Interest (ROI). Then to extract more effective features from the CXR images, the system utilized two feature extractors including HOG and LPQ descriptors to take two different feature vectors from the same image dataset. Next, combining these two features and used to train classification techniques with the entire training/test set as input data. Lastly, the ML classifiers performed included the SVM, KNN, Ensemble, DT and NB to categorize whether the patient is affected with covid or not. Figure 1 demonstrates the elementary stages of the recommended scheme architecture.

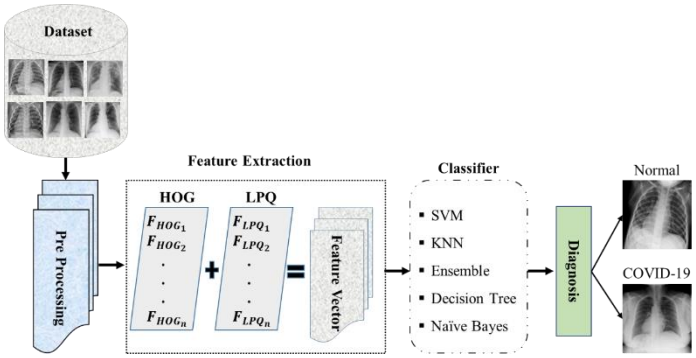

Figure 1: Workflow of the proposed system.

3.2 COVID-19 Dataset

The structure of the dataset is the primary stage in any computerized technique. Therefore, a dataset was created based on the COVID-19 Radiography Dataset that is a publicly available dataset. The dataset includes a total of 21165 CXR images, of which 10,192 are normal, 3616 are COVID-19 positive, 6012 are lung opacity (Non-COVID-19), and 1345 are viral pneumonia instances. The sample for this research consists of 7232 CXR images, 3616 of which have a positive COVID-19 identification and 3616 negatives that were chosen at random to produce the balanced dataset. The dataset contained various sizes of images and the sample CXR images of each class were given in Figure 2.

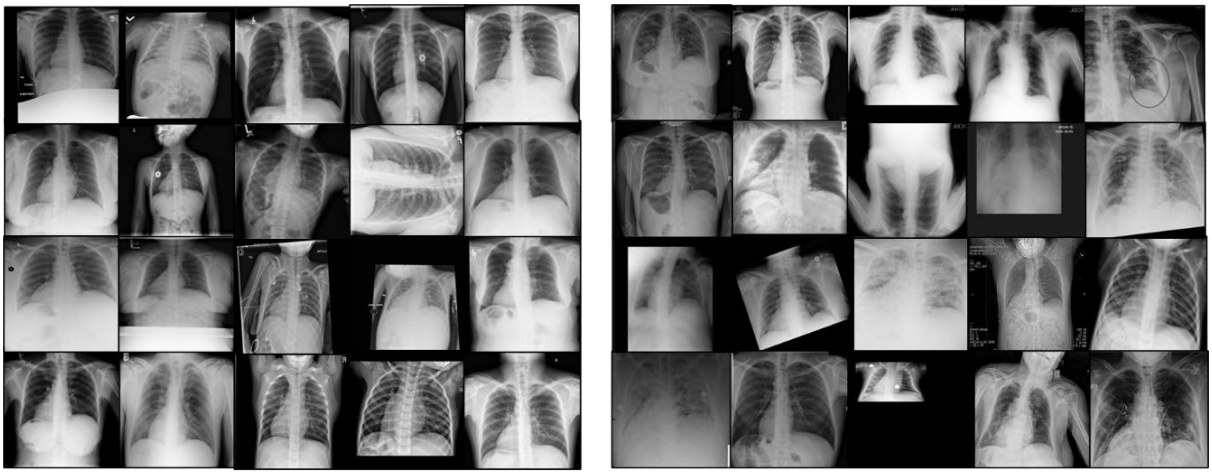

Figure 2: Examples of CXR images: (a) COVID-19, (b) Normal.

3.3 Preprocessing

Preparing images for use in model training and validation is referred to as image preprocessing. The act of transforming image data into a format that machine learning algorithms can understand is known as image data preparation. It's widely used to increase the model accuracy while also minimizing its complexities. There are several different methods used to preprocess image data. Proposed model applied preprocessing to all images in the dataset, first selecting the image's ROI and

resizing it to 512 X 512 pixels. Then, transformed the CXR images from RGB to grayscale as shown in Figure 3.

Figure 3: Preprocessing overall framework.

3.4 Feature Extraction

A series of experiments is the starting point for feature extraction, which then produces derived features that are meant to be valuable, making learning and adaptation easier and, in some circumstances, contribute to higher human interpretations. A reduced set of feature vectors could be generated from input data that is too large to analyze and process the dataset[24,25]. In the proposed scheme two different sorts of descriptors, namely HOG and LPQ feature extractors were utilized to derive features from the CXR images.

3.4.1 Histogram of Oriented Gradient (HOG)

According to a recommendation made by N. Dalal and B. Triggs, the HOG is utilized for object detection in computer vision and image processing[26]. It's a feature extraction technique for extracting features from image data that counts how many times a gradient direction occurs in a specific area of the image. HOG is implemented in four steps: first, at each region, extract a fixed-sized window and scale it; then, by combining the image's magnitude and angle, the image's gradient is computed. For each pixel in a 3x3 pixel block, the first Gx and Gy values are calculated using the formulae below.

$$G_x = I\,(C+1,R) - I\,(C-1,R) \quad (1)$$

$$G_y = I\,(R-1,C) - I\,(R+1,C) \quad (2)$$

Here, the symbols R and C stand for the rows and columns, respectively. Following the computation of Gx and Gy, each pixel's magnitude and angle are approximated using the formulas described below:

$$\text{Magnitude} = \sqrt{\left[G_x^2 + G_y^2\right]} \quad (3)$$

After computing the gradient, the direction can be computed as follows:

$$Tan^{-1}\,\emptyset \quad \text{where } \emptyset = \frac{G_x}{G_y} \quad (4)$$

where Ø characterizes the subsequent angle while Gx and GY are the elements along X and Y directions. Afterwards, a histogram of edge orientations is created using the gradients of the pixels in each cell[27–29]. Finally, once the histogram computation is ended, a combined feature is constructed to produce the HOG feature map, which comprises the encoding of the CXR images. In this work, HOG was utilized to derive a set of 81 features from a sample of CXR images for each image. Figure 4 shows how the HOG operator performs upon every image.

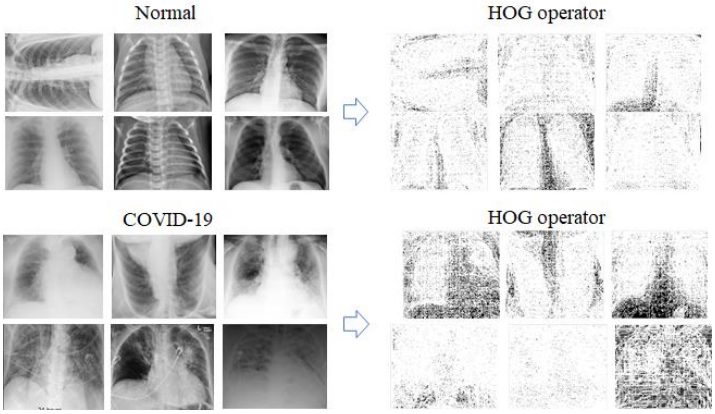

Figure 4: Example of feature extraction using HOG descriptor.

3.4.2 Local Phase Quantization (LPQ)

Ojansivu and Heikkila introduced the LPQ operator as a texture descriptor for the first time[30]. Blur invariance of the Fourier phase spectrum is the base for LPQ operator which uses 2-D Short-term Fourier Transform (STFT) calculations across a rectangle neighborhood at each pixel location to extract local phase information from the image[31]. Equation illustrates the STFT calculated at each pixel point x of the rectangle M by M neighborhood Nx of the image f(x) represented by this formula(5).

$$F\,(u,x) = \sum_{y\,\in N_x} F(x-y)e^{-j2\pi u^T y} = W_u^T fx \quad (5)$$

Where Wu is the 2-D DFT's base vector at frequency u, and fx is an additional vector comprising all M2 image samples from Nx. Only four complex coefficients are engaged into account in LPQ, $u1 = [a,0]T, u2 = [0,a]T, u3 = [a,a]T, u4 = [a,-a]T$, Where a is a scalar frequency below the first zero crossing of H(u) that meets a requirement of H(ui) > 0. As a result, this will lead to the creation of a vector for each pixel as displayed in Equation (6).

$$F_x = [\mathrm{F}\,(u_1,\mathrm{x}), \mathrm{F}\,(u_2,\mathrm{x}), \mathrm{F}\,(u_3,\mathrm{x}), \mathrm{F}\,(u_4,\mathrm{x})] \quad (6)$$

By evaluating the indications of each component's real and imaginary components in Fx. The Fourier coefficients can be used to record phase information. This is accomplished by employing the following simple scalar quantization equation (7).

$$q_i = \begin{cases} 1 & if\ g_i \geq 0 \\ 0 & otherwise \end{cases} \quad (7)$$

The binary coding pattern is represented by the eight binary coefficients qi. A decimal number between 0 and 255 will be generated from this code. The LPQ histogram will then have 256 bins[32]. In this work, LPQ was used to extract a set of 256 features for each image from the collection of CXR images. Figure 5 shows how the LPQ operator works for each image.

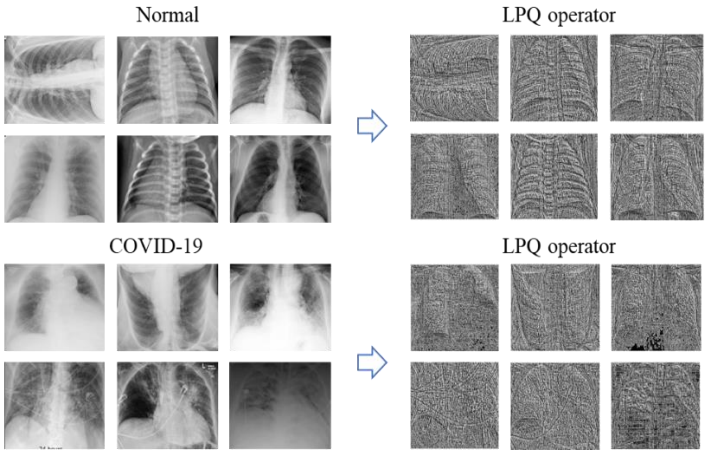

Figure 5: Example of feature extraction using LPQ descriptor.

3.5 Feature Fusion

The CXR images were used to derive the appropriate HOG and LPQ features. A new feature matrix was created by concatenating the two feature matrices, which was then the fused feature matrix feed into the machine learning algorithm for training and performing prediction on testing. The proposed model was used to classify the data into two categories either COVID or Non-COVID, and the results were compared to a single texture feature classification strategy, which was found to be more accurate and better in all metrics[24]. The extracted feature vectors were fused by concatenation and depicted in Figure (6).

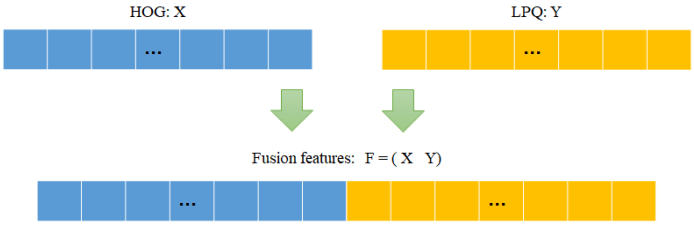

Figure 6: The procedure of the multi-feature fusion strategy.

3.6 Classifier and Performance Metrics

The suggested approach classifies the findings into two categories using ML classifiers, with each classifier yielding a distinct outcome. In this study, five different classification approaches have been used, namely, SVM, KNN, Ensemble, DT, and NB, as classifiers to classify the CXR images. In SVM executions, the kernel functions are linear, RBF, and polynomial; these kernels were utilized to know which kernel attained the best result and achieved the highest accuracy scores. A series of indicators, such as accuracy, precision, recall, specificity, F-score, MCC, and error rate measurements, have been computed to examine how well the three separate scenarios performed (see Table 1). The four output values that represent the outcome of the algorithm's prediction are referred to as a confusion matrix. There are two main parts: the positive part, which consists of True Positive (TP), False Positive (FP) and the second part, True Negative (TN), and False Negative (FN).

Table *1*: Performance metrics used in this study.

Metric	Formula
Accuracy	(TN+TP) / (TN+TP+FN+FP)
Precision	TP / (FP+TP)
Recall (Sensitivity)	TP / (FN+TP)
Specificity	TN / (FP+TN)
F-score	2(Rcall+Precision) / (Recall+Precision)
MCC	((TN×TP) -(FN×FP)) / ((TP+FP) ×(FN+TP)×FP×TN×(TN+FN))$^{0.5}$
Error Rate	(FN+FP) / (N+P)

4. Discussion of Experiment Results

The suggested model's performance was evaluated using extracted features generated from HOG and LPQ coefficients from over 7200 CXR to automatically identify the COVID-19 class. All experiments were carried out in the MATLAB programming environment. Various scenarios involving different features individually and combinations of HOG and LPQ features were suggested and analyzed. Five supervised ML classifiers (KNN, Ensemble, DT, NB and SVM with kernel) were performed to categorize derived features for each scenario in order to determine which scenario provided the best classification results. Additionally, the entire dataset was separated into two subgroups: 80% for training set and 20% for assessing performance of the classifier utilizing holdout cross-validation procedure. Accuracy, recall (sensitivity), precision, specificity, F1-score, and MCC metrics derived from the confusion matrix were calculated to evaluate the performance of the suggested scenarios.

From the experimentations executed on the COVID-19 Radiography dataset, all metrics were computed to estimate the performance of each scenario as (mean ± SD) with KNN (Table 2), Ensemble (Table 3), DT (Table 4), NB (Table 5), SVMP (Table 6), SVMRBF (Table 7), and SVML (Table 8) classifiers respectively. Conferring to the findings in Tables (2–7), it is determined that fusing the HOG and LPQ features (scenario 3) together reached the highest accuracy of 97.15 ± 0.38 % along with the SVMP classifier.

Based on the experiments conducted on the dataset Table (2), all matrices recorded the highest results in the fusion features compared to the features used individually. The performance metrics MCC, specificity, F-Score, precision, recall, and accuracy showed better results in fusion features with the KNN classifier which were 84.02 ± 1.61%, 89.57 ± 1.64%, 92.14 ± 0.76%, 94.34 ± 0.55%, 90.06 ± 1.39%, and 91.95 ± 0.83% respectively, compared to each HOG and LPQ feature separately.

When the Ensemble classifier was utilized, the findings observed that various types of features responded differently to predicted performance, as shown in Table (3). The fusion strategy was the

most potent for estimation, with an accuracy of 95.56 ± 0.57%, recall of 95.61 ± 0.79%, precision of 95.5 ± 0.61%, F-score of 95.55 ± 0.57%, specificity of 95.61 ± 0.81%, and MCC of 91.12 ± 1.15% compared to other feature extraction procedures.

Table *2*: Performance analysis based on KNN classifier. The bold marked values represent the best results obtained per metric.

Feature	Performance Metrics (%)					
	MCC	Specificity	F-Score	Precision	Recall	Accuracy
HOG	79.07 ± 1.33	86.26 ± 1.51	89.78 ± 0.61	92.64 ± 0.63	87.10 ± 1.20	89.45 ± 0.70
LPQ	79.32 ± 1.83	87.02 ± 1.82	89.87 ± 0.84	92.18 ± 0.57	87.68 ± 1.51	89.60 ± 0.94
HOG + LPQ	**84.02 ± 1.61**	**89.57 ± 1.64**	**92.14 ± 0.76**	**94.34 ± 0.55**	**90.06 ± 1.39**	**91.95 ± 0.83**

Table *3*: Performance analysis based on Ensemble classifier. The bold marked values represent the best results obtained per metric.

Feature	Performance Metrics (%)					
	MCC	Specificity	F-Score	Precision	Recall	Accuracy
HOG	83.76 ± 0.80	91.65 ± 0.98	91.89 ± 0.40	92.08 ± 0.90	91.7 ± 0.83	91.87 ± 0.40
LPQ	86.21 ± 1.40	93.58 ± 0.92	93.07 ± 0.69	92.62 ± 0.78	93.52 ± 0.88	93.1 ± 0.70
HOG + LPQ	**91.12 ± 1.15**	**95.61 ± 0.81**	**95.55 ± 0.57**	**95.5 ± 0.61**	**95.61 ± 0.79**	**95.56 ± 0.57**

According to the results revealed in Tables (4-5), the recommended HOG + LPQ strategy achieved the greatest performance result with all indicators utilizing the DT and NB classifiers. Conversely, DT and NB classifiers recorded the lowest performance scores in all the metrics among all the ML classifiers utilized in this study.

Table *4*: Performance analysis based on DT classifier. The bold marked values represent the best results obtained per metric.

Feature	Performance Metrics (%)					
	MCC	Specificity	F-Score	Precision	Recall	Accuracy
HOG	64.59 ± 1.92	81.53 ± 1.47	82.41 ± 0.96	83.04 ± 1.43	81.82 ± 1.18	82.28 ± 0.95
LPQ	69.36 ± 2.34	84.56 ± 1.36	84.68 ± 1.22	84.78 ± 1.76	84.6 ± 1.20	84.67 ± 1.17
HOG + LPQ	**71.34 ± 2.16**	**85 ± 2.25**	**85.75 ± 0.97**	**86.3 ± 1.01**	**85.23 ± 1.83**	**85.65 ± 1.09**

Table *5*: Performance analysis based on NB classifier. The bold marked values represent the best results obtained per metric.

Feature	Performance Metrics (%)					
	MCC	Specificity	F-Score	Precision	Recall	Accuracy
HOG	54.81 ± 1.81	72.28 ± 2.02	78.32 ± 0.92	82.22 ± 2.01	74.81 ± 1.18	77.25 ± 0.89
LPQ	60.6 ± 1.92	74.45 ± 2.23	81.16 ± 0.83	85.73 ± 1.19	77.07 ± 1.43	80.09 ± 1.02
HOG + LPQ	**62.34 ± 1.28**	**76.52 ± 1.71**	**81.96 ± 0.89**	**85.78 ± 1.1**	**78.49 ± 1.07**	**81.03 ± 0.67**

Tables (6-8) contain a list of all the SVM models' performance outcomes. Based on the investigational consequences for all three scenarios, it can be confirmed that the features combined from the HOG and LPQ techniques performed better than the other scenarios using the SVMP, SVML, and SVMRBF classifiers. Results demonstrated that the proposed fusion scheme demonstrated greater than other options when comparing the SVMP, SVML, and SVMRBF models, and achieved the highest overall accuracy of 97.15 ± 0.38% with the SVM classifier using polynomial kernel. Other performance metrics (recall, precision, F-Score, Specificity, and MCC) have been found to be 96.65 ± 0.62, 96.4 ± 0.60, 96.52 ± 0.28, 96.65 ± 0.66 and 93.06 ± 0.57, respectively.

Depending on the experimental outcomes depicted in Figure (7), it can be determined that combining features generated from HOG and LPQ approaches improves performance and outperformed the other two scenarios with all metrics in this study. The fusion procedure had a higher probability of having a

better outcome. However, the fusion technique with the SVMP classifier have delivered an extremely maximum average accuracy of 97.15 ± 0.38% among the remaining classifiers for all scenarios.

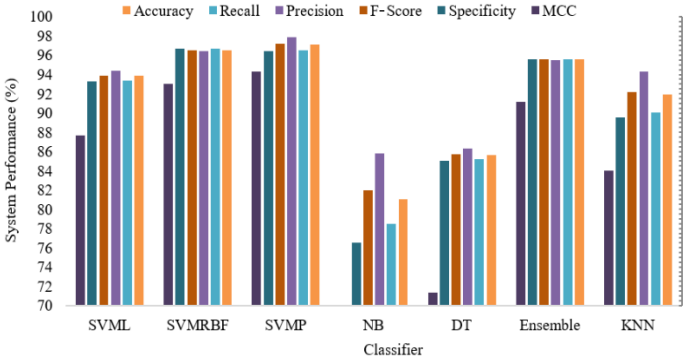

Figure 7: Display accuracy in all machine learning classifiers.

The misclassification error rate indicator was included in this work to evaluate the performance of the suggested scenarios, as revealed in Figure (8). The consequences presented that combining HOG and LPQ feature sets to the SVM classifier with a polynomial kernel produced a lowest misclassification error of 2.85%, demonstrating that the suggested scenario operates significantly better than earlier suggested scenarios. As a consequence, the fusion scenario was taken into account as a potential method for identifying Covid-19 CXR images. Finally, as shown in Table (9), the suggested fusion scheme's performance was compared to some of the recent existing methods. The suggested system produced impressive results when compared to existing methods, particularly in terms of average classification accuracy. This is attributable to the HOG-LPQ methods and SVMP classifier working together, which allowed them to gain their advantages. Furthermore, the proposed technique utilized 337 features to achieve the best results with a 97.15 %, which yielded the greatest performance results when compared to the other researchers' usage of a large number of features.

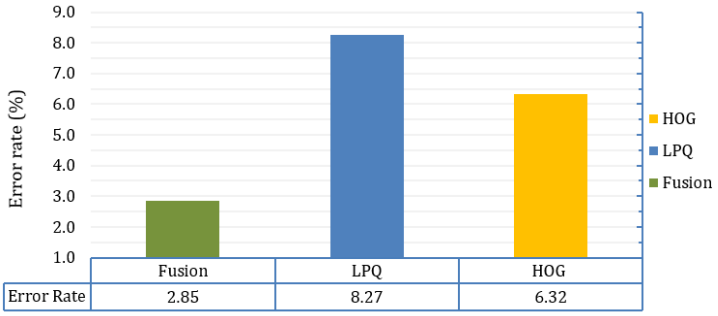

Figure 8: Misclassification error rate for different scenarios using SVMP classifier.

Table 6: Performance analysis based on SVMP classifier. The bold marked values represent the best results obtained per metric.

Feature	Performance Metrics (%)					
	MCC	Specificity	F-Score	Precision	Recall	Accuracy
HOG	87.38 ± 1.59	92.66 ± 1.01	93.74 ± 0.79	94.68 ± 1.21	92.82 ± 0.92	93.67 ± 0.79
LPQ	90.2 ± 1.22	94.5 ± 0.93	95.12 ± 0.59	95.68 ± 0.57	94.57 ± 0.87	95.09 ± 0.61
HOG + LPQ	**94.31 ± 0.76**	**96.45 ± 0.85**	**97.17 ± 0.38**	**97.84 ± 0.62**	**96.51 ± 0.79**	**97.15 ± 0.38**

Table 7: Performance analysis based on SVMRBF classifier. The bold marked values represent the best results obtained per metric.

Feature	Performance Metrics (%)					
	MCC	Specificity	F-Score	Precision	Recall	Accuracy
HOG	87.51 ± 1.11	93.6 ± 0.65	93.76 ± 0.58	93.9 ± 1.15	93.63 ± 0.59	93.75 ± 0.55
LPQ	89.39 ± 1.10	95.14 ± 0.57	94.67 ± 0.55	94.24 ± 0.61	95.1 ± 0.56	94.69 ± 0.55
HOG + LPQ	**93.06 ± 0.57**	**96.65 ± 0.66**	**96.52 ± 0.28**	**96.4 ± 0.60**	**96.65 ± 0.62**	**96.52 ± 0.28**

Table 8: Performance analysis based on SVML classifier. The bold marked values represent the best results obtained per metric.

Feature	Performance Metrics (%)					
	MCC	Specificity	F-Score	Precision	Recall	Accuracy
HOG	77.48 ± 1.24	88.07 ± 0.76	88.8 ± 0.69	89.39 ± 1.48	88.23 ± 0.58	88.73 ± 0.61
LPQ	83.48 ± 1.35	91.03 ± 1.42	91.78 ± 0.65	92.42 ± 1.04	91.17 ± 1.25	91.72 ± 0.68
HOG + LPQ	**87.71 ± 1.51**	**93.31 ± 1.19**	**93.88 ± 0.73**	**94.38 ± 0.78**	**93.4 ± 1.10**	**93.85 ± 0.75**

Table 9: Comparison of proposed classification accuracy with existing state-of-the-art techniques.

Previous study	Data type	Number of Class	Year	Methods/ classifier	Accuracy (%)
A. I. Khan et al[33]	X-Ray	4	2020	(CNN) CoroNet	89.60
A. Afifi et al[34]	X-Ray	3	2021	DenseNet161	91.20
A. Zargari Khuzani et al[35]	X-Ray	2	2021	ResNet-18	92.49
L. Wang et al[36]	X-Ray	3	2020	COVID-Net	93.30
M. Owais et al[37]	CT-scan and X-Ray	2	2021	Ensemble-Net	94.72
F. Saiz and I. Barandiaran[14]	X-Ray	2	2020	SDD300	94.92
P. K. Sethy et al[15]	X-Ray	3	2020	ResNet50 + SVM	95.33
F. H. Ahmad and S. H. Wady[22]	X-Ray	2	2021	SVM (CT+GWT+LGIP)	96.18
Proposed	**X-Ray**	**2**	**2022**	**SVMP (HOG +LPQ)**	**97.15 ± 0.38**

5. Conclusion

COVID-19 patients must be diagnosed early to prevent the disease from spreading to others. The key objective of the recommended model in this paper is to predict COVID-19 patients utilizing CXR images. Therefore, A fusion approach was suggested based on the combined features of HOG and LPQ approaches as well as a ML method for diagnosing Covid-19 cases. The experiments used a balanced dataset of 7232 CXR images collected from a COVID-19 Radiography dataset as training and testing data. Each trained model was assessed using benchmark evaluating performance with accuracy, specificity, recall, precision, F1-score, MCC, and error rate metrics in three various scenarios involving different classifiers. Experimental results show that combined HOG-LPQ model with SVMP classifier yielded the highest performance measures (accuracy = 97.15 ± 0.38%, precision = 96.51 ± 0.79%, recall = 97.84 ± 0.62%, specificity = 97.17 ± 0.38%, F1-score = 96.45 ± 0.85%, MCC = 94.31 ± 0.76%). Due to the obvious improved performance, it is expected that research findings would assist radiologists in formulating clinical decisions. In further studies, the classification performance can be investigated by utilizing different feature extraction methods and feature selection models with the Neutrosophic theory.

Acknowledgements

The authors acknowledge the participants for their time and answering the questionnaire

Conflict of interests

None

References

[1] Nur-a-alam, M. Ahsan, M. A. Based, J. Haider, and M. Kowalski, "COVID-19 detection from chest X-ray images using feature fusion and deep learning," *Sensors*, vol. 21, no. 4, pp. 1–30, 2021, doi: 10.3390/s21041480.

[2] S. B. Desai, A. Pareek, and M. P. Lungren, "Deep learning and its role in COVID-19 medical imaging," *Intell. Med.*, vol. 3–4, no. October, p. 100013, 2020, doi: 10.1016/j.ibmed.2020.100013.

[3] N. K. Jha *et al.*, "β-Caryophyllene, A Natural Dietary CB2 Receptor Selective Cannabinoid can be a Candidate to Target the Trinity of Infection, Immunity, and Inflammation in COVID-19," *Front. Pharmacol.*, vol. 12, no. May, pp. 1–24, 2021, doi: 10.3389/fphar.2021.590201.

[4] S. Asif, Y. Wenhui, H. Jin, and S. Jinhai, "Classification of COVID-19 from Chest X-ray images using Deep Convolutional Neural Network," *2020 IEEE 6th Int. Conf. Comput. Commun. ICCC 2020*, no. March 2020, pp. 426–433, 2020, doi: 10.1109/ICCC51575.2020.9344870.

[5] A. Tchagna Kouanou *et al.*, "An Overview of Supervised Machine Learning Methods and Data Analysis for COVID-19 Detection," *J. Healthc. Eng.*, vol. 2021, 2021, doi: 10.1155/2021/4733167.

[6] S. A. J. Zaidi, S. Tariq, and S. B. Belhaouari, "Future prediction of covid-19 vaccine trends using a voting classifier," *Data*, vol. 6, no. 11, 2021, doi: 10.3390/data6110112.

[7] M. Turkoglu, "COVIDetectioNet: COVID-19 diagnosis system based on X-ray images using features selected from pre-learned deep features ensemble," *Appl. Intell.*, vol. 51, no. 3, pp. 1213–1226, 2021, doi: 10.1007/s10489-020-01888-w.

[8] T. Ilyas, D. Mahmood, G. Ahmed, and A. Akhunzada, "Symptom analysis using fuzzy logic for detection and monitoring of covid-19 patients," *Energies*, vol. 14, no. 21, 2021, doi: 10.3390/en14217023.

[9] L. Chen *et al.*, "Identifying COVID-19-Specific Transcriptomic Biomarkers with Machine Learning Methods," *Biomed Res. Int.*, vol. 2021, 2021, doi: 10.1155/2021/9939134.

[10] S. Hira, A. Bai, and S. Hira, "An automatic approach based on CNN architecture to detect Covid-19 disease from chest X-ray images," *Appl. Intell.*, vol. 51, no. 5, pp. 2864–2889, 2021, doi: 10.1007/s10489-020-02010-w.

[11] S. S. Aljameel, I. U. Khan, N. Aslam, M. Aljabri, and E. S. Alsulmi, "Machine Learning-Based Model to Predict the Disease Severity and Outcome in COVID-19 Patients," *Sci. Program.*, vol. 2021, 2021, doi: 10.1155/2021/5587188.

[12] A. Davoudi *et al.*, "Studying the Effect of Taking Statins before Infection in the Severity Reduction of COVID-19 with Machine Learning," *Biomed Res. Int.*, vol. 2021, 2021, doi: 10.1155/2021/9995073.

[13] A. K. Singh, A. Kumar, M. Mahmud, M. S. Kaiser, and A. Kishore, "COVID-19 Infection Detection from Chest X-Ray Images Using Hybrid Social Group Optimization and Support Vector Classifier," *Cognit. Comput.*, no. 0123456789, 2021, doi: 10.1007/s12559-021-09848-3.

[14] F. Saiz and I. Barandiaran, "COVID-19 Detection in Chest X-ray Images using a Deep Learning Approach," *Int. J. Interact. Multimed. Artif. Intell.*, vol. 6, no. 2, p. 4, 2020, doi: 10.9781/ijimai.2020.04.003.

[15] P. K. Sethy, S. K. Behera, P. K. Ratha, and P. Biswas, "Detection of coronavirus disease (COVID-19) based on deep features and support vector machine," *Int. J. Math. Eng. Manag. Sci.*, vol. 5, no. 4, pp. 643–651, 2020, doi: 10.33889/IJMEMS.2020.5.4.052.

[16] A. Narin, C. Kaya, and Z. Pamuk, "Automatic detection of coronavirus disease (COVID-19) using X-ray images and deep convolutional neural

networks," *Pattern Anal. Appl.*, vol. 24, no. 3, pp. 1207–1220, 2021, doi: 10.1007/s10044-021-00984-y.

[17] V. N. M. Aradhya, M. Mahmud, D. S. Guru, B. Agarwal, and M. S. Kaiser, "One-shot Cluster-Based Approach for the Detection of COVID–19 from Chest X–ray Images," *Cognit. Comput.*, vol. 13, no. 4, pp. 873–881, 2021, doi: 10.1007/s12559-020-09774-w.

[18] D. Ji, Z. Zhang, Y. Zhao, and Q. Zhao, "Research on Classification of COVID-19 Chest X-Ray Image Modal Feature Fusion Based on Deep Learning," *J. Healthc. Eng.*, vol. 2021, 2021, doi: 10.1155/2021/6799202.

[19] S. V J and J. F. D, "Deep Learning Algorithm for COVID-19 Classification Using Chest X-Ray Images," *Comput. Math. Methods Med.*, vol. 2021, p. 9269173, 2021, doi: 10.1155/2021/9269173.

[20] T. S. Qaid, H. Mazaar, M. Y. H. Al-shamri, M. S. Alqahtani, A. A. Raweh, and W. Alakwaa, "Hybrid Deep-Learning and Machine-Learning Models for Predicting COVID-19," vol. 2021, 2021.

[21] E. G. Moung, C. J. Hou, M. M. Sufian, M. H. A. Hijazi, J. A. Dargham, and S. Omatu, "Fusion of moment invariant method and deep learning algorithm for COVID-19 classification," *Big Data Cogn. Comput.*, vol. 5, no. 4, 2021, doi: 10.3390/bdcc5040074.

[22] F. H. Ahmad and S. H. Wady, "COVID-19 Infection Detection from Chest X-Ray Images Using Feature Fusion and Machine Learning," *Sci. J. Cihan Univ. – Sulaimaniya*, vol. 5, no. 2, pp. 10–30, 2021.

[23] A. M. Ismael and A. Şengür, "Deep learning approaches for COVID-19 detection based on chest X-ray images," *Expert Syst. Appl.*, vol. 164, p. 114054, 2021, doi: 10.1016/j.eswa.2020.114054.

[24] J. Chen, Y. Zhang, and Y. Jiang, "Multi-features fusion classification method for texture image," *J. Eng.*, vol. 2019, no. 23, pp. 8834–8838, 2019, doi: 10.1049/joe.2018.9118.

[25] A. Humeau-Heurtier, "Texture feature extraction methods: A survey," *IEEE Access*, vol. 7, no. c, pp. 8975–9000, 2019, doi: 10.1109/ACCESS.2018.2890743.

[26] J. Shin, D. Kim, and C. Ruland, "Content based image authentication using HOG feature descriptor," *2014 IEEE Int. Conf. Image Process. ICIP 2014*, pp. 5292–5296, 2014, doi: 10.1109/ICIP.2014.7026071.

[27] M. Davis and F. Sahin, "HOG feature human detection system," *2016 IEEE Int. Conf. Syst. Man, Cybern. SMC 2016 - Conf. Proc.*, pp. 2878–2883, 2017, doi: 10.1109/SMC.2016.7844676.

[28] R. Kapoor, R. Gupta, L. H. Son, S. Jha, and R. Kumar, "Detection of Power Quality Event using Histogram of Oriented Gradients and Support Vector Machine," *Meas. J. Int. Meas. Confed.*, vol. 120, pp. 52–75, 2018, doi: 10.1016/j.measurement.2018.02.008.

[29] T. Kobayashi, A. Hidaka, and T. Kurita, "Selection of Histograms of Oriented Gradients," *Int. Conf. ICONIP*, pp. 598–607, 2008.

[30] A. Chergui, S. Ouchtati, and F. Bougourzi, "LPQ and LDP Descriptors with ML Representation For Kinship verification," *Int. Work. Signal Process. Appl. to Rotating Mach. Diagnostics*, vol. 2, no. April, 2018.

[31] J. Heikkilä and V. Ojansivu, "Methods for local phase quantization in blur-insensitive image analysis," *2009 Int. Work. Local Non-Local Approx. Image Process. LNLA 2009*, no. 2, pp. 104–111, 2009, doi: 10.1109/LNLA.2009.5278397.

[32] S. Brahnam, L. Nanni, J. Shi, and A. Lumini, "Local phase quantization texture descriptor for protein classification," *Int. Conf. Bioinforma. Comput. Biol.*, pp. 159–165, 2010.

[33] A. I. Khan, J. L. Shah, and M. M. Bhat, "CoroNet: A deep neural network for detection and diagnosis of COVID-19 from chest x-ray images," *Comput. Methods Programs Biomed.*, vol. 196, p. 105581, 2020, doi: 10.1016/j.cmpb.2020.105581.

[34] A. Afifi, N. E. Hafsa, M. A. S. Ali, A. Alhumam, and S. Alsalman, "An ensemble of global and local-attention based convolutional neural networks for COVID-19 diagnosis on chest X-ray images," *Symmetry (Basel).*, vol. 13, no. 1, pp. 1–25, 2021, doi: 10.3390/sym13010113.

[35] A. Zargari Khuzani, M. Heidari, and S. A. Shariati, "COVID-Classifier: an automated machine learning model to assist in the diagnosis of COVID-19 infection in chest X-ray images," *Sci. Rep.*, vol. 11, no. 1, pp. 1–6, 2021, doi: 10.1038/s41598-021-88807-2.

[36] L. Wang, Z. Q. Lin, and A. Wong, "COVID-Net: a tailored deep convolutional neural network design for detection of COVID-19 cases from chest X-ray images," *Sci. Rep.*, vol. 10, no. 1, pp. 1–12, 2020, doi: 10.1038/s41598-020-76550-z.

[37] M. Owais, H. S. Yoon, T. Mahmood, A. Haider, H. Sultan, and K. R. Park, "Light-weighted ensemble network with multilevel activation visualization for robust diagnosis of COVID19 pneumonia from large-scale chest radiographic database," *Appl. Soft Comput.*, vol. 108, no. April, p. 107490, 2021, doi: 10.1016/j.asoc.2021.107490.